University of Liège

Departement of Astrophysics, Geophysics et Oceanography
Astrophysics et Geophysics Institut

Innovative techniques to find strongly lensed systems

Laisney Clément

1. Promotor Sluse Dominique
Cosmologics et Astrophysics Origins
University of Liège

2. Promotor Delchambre Ludovic
Group of AstroPhysics and High-Energies
University of Liège

June 2023

Abstract

Acknowledgement

Contents

1 Introduction

A gravitational lens, also known as a cosmic mirage, is a distribution of mass able to bend the light coming from a distant source. This phenomenon is similar to a light beam bent through a lens by refraction. This is why we call it gravitational lensing.

Already in 1704, Isaac Newton speculated that "[...] Bodies act upon Light at a distance, and by their action bend its Rays; and [...] this action [is] strongest at the least distance." [1]. Later John Mitchell proposed to Henry Cavendish, a method to measure the mass of stars by detecting a reduction of the speed of light affected by gravity [2]. In those letters, Mitchell suggested that a massive enough body could stop the light: a black hole. This pushed Cavendish to calculate the Newtonian light deflection. Unfortunately, he never published his manuscript dated around 1784 [3]. Johann Georg von Soldner published the same result in 1801 [4] assuming the light is a corpuscle. Finally, Einstein calculated the same value thanks to the equivalence principle only in 1911 [5] and corrected it by twice the value in 1915 [6] in the frame of General Relativity.

The first observation of light deflection was performed in 1919 by Arthur Eddington and Frank Watson Dyson by observing a change in the position of stars near the sun during the solar eclipse of May 29 [7]. Later in 1937, after the new discovery of Galaxies, Fritz Zwicky speculated that those massive objects could act as both source and lens with a larger effect much likely to be observed [8]. It was necessary to wait until 1979 to observe the first gravitational lens. Dennis Walsh, Bob Carswell, and Ray Weysmann observed two identical QuasiStellar Objects (QSO) using Kitt Peak National Observatory. The difficulties in describing them as two distinct objects were highlighted in their paper [9], along with the discussion of the hint suggesting the observation of two images of the same object formed through gravitational lensing. SBS 0957+561 was renamed "Twin QSO".

1.1 Scientific context

Lenses used to be serendipitously found, but nowadays we are looking for gravitational lenses in large amounts thanks to large survey programs. One can cite an early example of systematic research of gravitational lenses: the Cosmic Lens All-Sky Survey (CLASS). Twenty-two lensed systems were found using the Very Large Array (VLA) radio telescope [10].

We generally subdivide lensing into 3 categories: Strong, Weak, and Micro-lensing. Strong lensing is the case where distortion of the background source is clearly identified or multiple lensed images are detected. For weak lensing, distortion is much smaller, and statistical studies are needed in order to find a distortion of about a few percent. The microlensing does not show any distortion but a variation of the background source light over time. The lensing object in a microlensing case may be a star while strong and weak lenses are typically galaxies or even galaxy clusters. Microlensing is often used to detect exoplanets [11]. In this work, I will focus on strongly lensed systems.

Studying gravitational lenses has a huge scientific interest. As F. Zwicky already mentioned in his paper in 1937 [8], they constitute a good source to test general relativity, they enable us to observe very distant galaxies and they allow us to determine masses of galaxies. In fact, it has many more applications like the determination of cosmological parameters (Ω_0: density parameter, λ_0: cosmological constant, and H_0: the Hubble constant). But the two main fields of interest are the study of dark matter and dark energy [12] [13], and modern cosmology [14] by better-determining cosmological distance scales, large-scale matter distribution, mass distribution in galaxy clusters, physics of quasars and galaxy structure.

With the rise of Large surveys and their ability to store a large amount of data, we are facing Big Data problems. As an example, the Euclid Consortium website[1] asserts that during the 6-year-long mission, Euclid will collect more than 500,000 visible and Near-Infrared images. In addition to that, ground-based telescopes will cover the same sky as Euclid in 4 different filters which represent a total of 7 different filters. This forms several millions of images that weigh 30 PetaByte of data. About 10 billion galaxies will be imaged during the mission. Other surveys like DES[2] (Dark Energy Survey) or LSST[3] deal with the same amount of data. About 700 million sources in the last DES data release and 2 million images (60 PetaByte) for

[1] https://www.euclid-ec.org/?page_id=2625
[2] https://www.darkenergysurvey.org/
[3] https://www.lsst.org/

LSST. Processing this tremendous amount of data requires detecting lensed systems autonomously. Moreover, the estimated occurrence of galaxy-galaxy strong lensing is 10^{-5}[15][16]. In most optimistic forecasts, DES, LSST, and Euclid can discover up to 2300, 120000, and 280000 lenses respectively[15]. The low occurrence of the phenomenon forces us to build observational and computational strategies to maximize the chances of detection. The common strategy adopted Today is the rise of lens candidates from survey data to be followed up later by dedicated ground-based telescopes. Because observation time is precious we clearly see the need for a robust autonomous model rising the least possible false positive cases.

1.2 Physics of Gravitational lenses

This section will focus on the mathematical demonstration of the gravitational lensing phenomenon. To do so, my development is largely inspired by Jean-François Claeskens and Jean Surdej's review [17] and Pierre Magain's lecture [18].

1.2.1 The Refraction analogy

As said earlier, J. von Soldner calculated the deviation angle of light by a spherical mass M thanks to Newton's theory of gravitation. This deviation angle $\alpha = \frac{2GM}{c^2 b}$ (where G is the gravitational constant, c the speed of light, and b the impact parameter.) was corrected later by Einstein thanks to general relativity. In this part, we will study gravitational lenses in the frame of General relativity.

Gravitational mirages are analogs of atmospheric mirages. This phenomenon arises when light trajectories are curved (scheme in fig 1.1) which is a consequence of an anisotropic speed of light along the light path. According to refraction laws, light rays are bent in an inhomogeneous medium. This is why we can approach this problem as a refraction problem, with light traveling from vacuum to a material medium of refraction index n_ϕ. The refractory analog situation is summarized in fig 1.2.

In vacuum; the speed of light is c, but in a material medium it becomes $v = \frac{c}{n_\phi}$. As a consequence of General relativity, spacetime is curved by a gravitational potential ϕ associated with a massive object. In the weak field approximation ($\frac{\phi}{c^2} \ll 1$), the metric is :

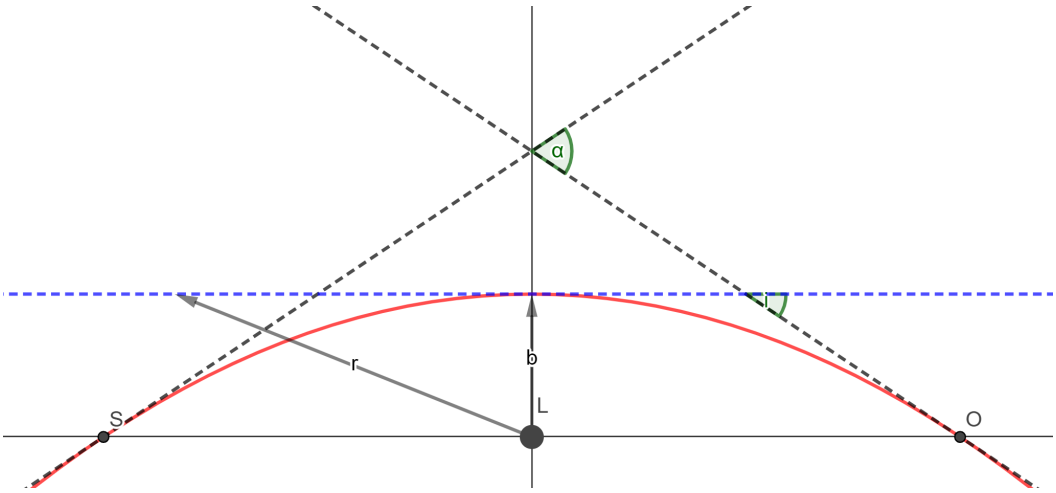

Fig. 1.1.: Deflection of light coming from a distant source (S) in the vicinity of a massive object (Lens: L) seen by the observer (O).

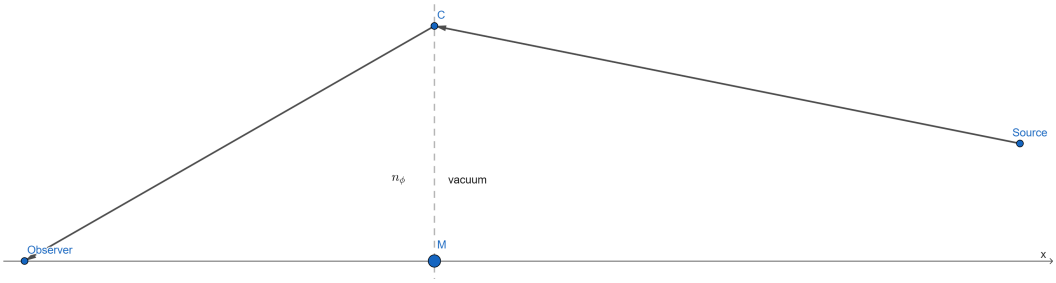

Fig. 1.2.: Analog situation of light traveling in vacuum from a distant source and propagating through a medium of refraction index n_ϕ.

$$ds^2 = -\left(1 + \frac{2\phi}{c^2}\right) c^2 dt^2 + \left(1 - \frac{2\phi}{c^2}\right) (dx^2 + dy^2 + dz^2) \tag{1.1}$$

As the light follows null geodesic, we have that $ds^2 = 0$ such that:

$$\left(1 + \frac{2\phi}{c^2}\right) c^2 dt^2 = \left(1 - \frac{2\phi}{c^2}\right) (dx^2 + dy^2 + dz^2) \tag{1.2}$$

$$dt^2 = \frac{1 - \frac{2\phi}{c^2}}{1 + \frac{2\phi}{c^2}} \frac{(dx^2 + dy^2 + dz^2)}{c^2} \tag{1.3}$$

$$dt^2 \approx \left(1 - \frac{2\phi}{c^2}\right)^2 \frac{(dx^2 + dy^2 + dz^2)}{c^2} \tag{1.4}$$

$$dt \approx \left(1 - \frac{2\phi}{c^2}\right) \frac{\sqrt{dx^2 + dy^2 + dz^2}}{c} \tag{1.5}$$

$$\frac{\sqrt{dx^2 + dy^2 + dz^2}}{dt} \approx \frac{c}{\left(1 - \frac{2\phi}{c^2}\right)} \tag{1.6}$$

equation 1.6 is analog to $v = \frac{c}{n_\phi}$. We identify $n_\phi = 1 - \frac{2\phi}{c^2}$. That being said, let's establish the lens equation and the deflection angle.

1.2.2 The lens equation

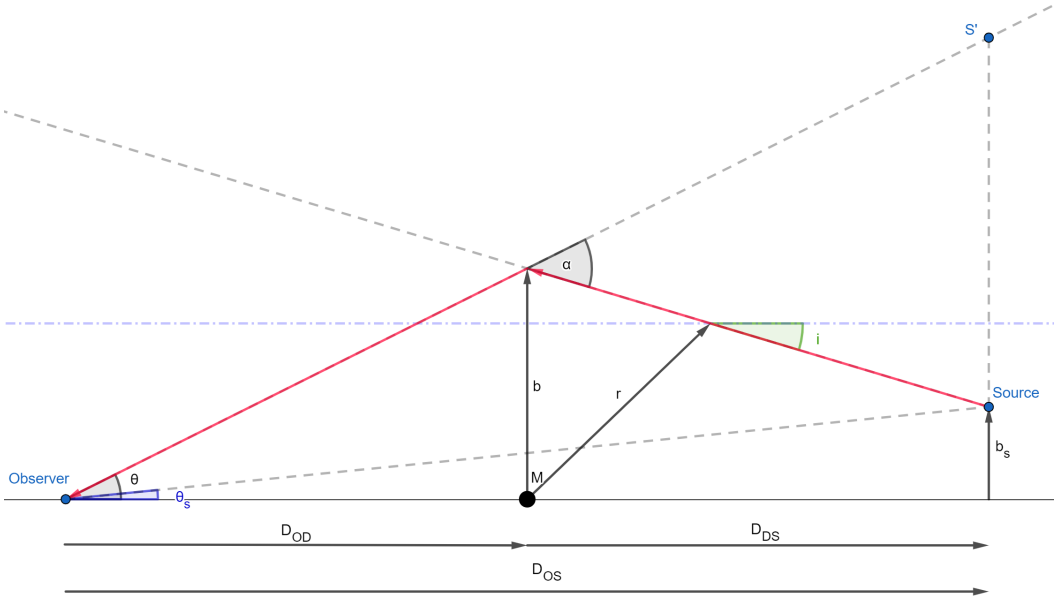

Fig. 1.3.: Scheme of the general situation of a gravitational lens

To solve this problem we need to link the viewing angle θ to the deflection angle α. By geometric considerations thanks to figure 1.3 this relation is given by the following equation :

$$\theta_s = \theta - \frac{D_{DS}}{D_{OS}}\alpha(b) \tag{1.7}$$

$$b = D_{OD}\theta \tag{1.8}$$

Now we have to link the deflection angle α to physical parameters like the mass of the deflector M. In the following, $\frac{di}{dx}$ is the variation of the direction along the x-axis.

α is thus the deflection angle which is the integration of all direction variations along x.

$$\alpha(b) = -\int_{-\infty}^{\infty} \frac{di}{dx} dx = -\int_{-\infty}^{\infty} \frac{1}{n_\phi} \frac{dn_\phi}{db} dx = \frac{2}{c^2} \int_{-\infty}^{\infty} \frac{d\phi}{db} dx \tag{1.9}$$

In this demonstration, we will take as a simple example a point mass deflector. Its gravitational potential is :

$$\phi = -\frac{GM}{r} = -\frac{GM}{\sqrt{b^2 + x^2}} \tag{1.10}$$

The deflection angle α becomes:

$$\alpha(b) = \frac{4GM}{c^2 b} \tag{1.11}$$

We effectively find twice the value obtained with the Newtonian framework. Now that we find what Einstein predicted, let's generalize. To do so, we use the thin lens approximation. This approximation allows us to describe a deflector by its surface mass density $\Sigma(\overrightarrow{b})$ projected in the deflector plane. The deflection angle is then expressed by :

$$\overrightarrow{\alpha}(\overrightarrow{b}) = \frac{4G}{c^2} \int_S \frac{\Sigma(\overrightarrow{b'})(\overrightarrow{b} - \overrightarrow{b'}) db'_1 db'_2}{|\overrightarrow{b} - \overrightarrow{b'}|^2} \tag{1.12}$$

In the case of a circularly symmetric mass distribution, with $M(b)$ the mass inside the radius b and $b = \| \overrightarrow{b} \|$:

$$\overrightarrow{\alpha}(\overrightarrow{b}) = \frac{4GM(b)}{c^2 b^2} \overrightarrow{b} \tag{1.13}$$

1.2.3 Einstein Ring

Let's now assume the following circularly symmetric lens mass distribution with M_0, the mass inside a radius b_0:

$$M(b) = M_0 \left(\frac{b}{b_0} \right)^\beta \tag{1.14}$$

$\beta = 0$ correspond to a point mass distribution, $\beta = 1$ is the singular isothermal sphere distribution and $\beta = 2$ yield the uniform distribution of matter.

Now that we have the general case, let's study a particular case which is the Einstein ring solution. This case corresponds to the simple case when the observer, the

deflector, and the source are aligned ($\theta_s = 0$). The Einstein ring is thus defined by its angular size θ_E. From equations 1.7, 1.13 and 1.14 we have that:

$$0 = \theta_E - \frac{D_{DS}}{D_{OS}} \frac{4GM(b)}{c^2 b} = \theta_E - \frac{D_{DS}}{D_{OS}} \frac{4G}{c^2 b} M_0 \left(\frac{b}{b_0}\right)^{\beta} \tag{1.15}$$

$$0 = \theta_E - \frac{D_{DS}}{D_{OS}} \frac{4GM_0}{c^2 b_0^{\beta}} \left(D_{OD}\theta_E\right)^{\beta-1} = \theta_E \left(1 - \frac{D_{DS}}{D_{OS}} \frac{4GM_0}{c^2 b_0^{\beta}} D_{OD}^{\beta-1} \theta_E^{\beta-2}\right) \tag{1.16}$$

$\theta_E = 0$ is a solution but not relevant.

$$\frac{D_{DS} D_{OD}^{\beta-1}}{D_{OS}} \frac{4GM_0}{c^2 b_0^{\beta}} \theta_E^{\beta-2} = 1 \tag{1.17}$$

$$\theta_E = \left(\frac{4GM_0}{c^2 b_0^{\beta}} \frac{D_{DS}}{D_{OD}^{1-\beta} D_{OS}}\right)^{\frac{1}{2-\beta}} \tag{1.18}$$

with M_E the mass inside the radius $b_E = D_{OD}\theta_E$ we get the expression of the Einstein ring angular size:

$$\theta_E = \sqrt{\frac{4GM_E}{c^2} \frac{D_{DS}}{D_{OD} D_{OS}}} \tag{1.19}$$

1.2.4 Images positions

By tacking a point mass deflector ($M(b) = M_0$):

$$\theta_s = \theta - \frac{D_{DS}}{D_{OS}} \frac{4GM_0}{c^2 b} = \theta - \frac{D_{DS}}{D_{OS}} \frac{4GM_0}{c^2 D_{OD} \theta} \tag{1.20}$$

$$\theta\theta_s = \theta^2 - \frac{D_{DS}}{D_{OS} D_{OD}} \frac{4GM_0}{c^2} \tag{1.21}$$

with $M_E = M_0$

$$\theta^2 - \theta_s \theta - \theta_E^2 = 0 \tag{1.22}$$

we are in the presence of a second-order polynomial with a determinant $\delta = \theta_s^2 + 4\theta_E^2 > 0$ and its two solutions:

$$\theta_{1,2} = \frac{1}{2}\left(\theta_s \pm \sqrt{\theta_s^2 + 4\theta_E^2}\right) \tag{1.23}$$

Let's now study two interesting properties. By considering a small misalignment ϵ between the source, the lens, and the observer; at first order, the angular separation of the image $\Delta\theta$ is:

$$\theta_1 = \frac{1}{2}\left(\epsilon + \sqrt{\epsilon^2 + 4\theta_E^2}\right) = \frac{1}{2}\epsilon + \frac{1}{2}\sqrt{4\theta_E^2} = \frac{1}{2}\epsilon + \theta_E \tag{1.24}$$

$$\theta_2 = \frac{1}{2}\epsilon - \theta_E \tag{1.25}$$

$$\Delta\theta = \theta_1 - \theta_2 = 2\theta_E \tag{1.26}$$

This means that the angular separation between 2 images increases with the mass of the deflector or increases when the deflector is closer to the observer.

The second property is about the mean surface density within θ_E which remains constant. We define this quantity as the critical surface mass density:

$$\bar{\Sigma}(\theta_E) \equiv \frac{M_E}{\pi(D_{OD}\theta_E)^2} = \frac{c^2 D_{OS}}{4\pi G D_{OD} D_{DS}} \equiv \Sigma_{crit} \tag{1.27}$$

This property implies that a finite massive object is a gravitational lens that produces multiple images if its central mass density $\Sigma > \Sigma_{crit}$

1.2.5 Magnification

Another property of gravitational lenses is the magnification. This quantity μ is given by the ratio between the surface brightness of the image and the source. In the following, we will stay in a 1D case but the magnification can be generalized using Jacobian given by this definition:

$$\mu = \frac{d\Omega_{image}}{d\Omega_{source}} = \left| det\left(\frac{\partial\theta_s}{\partial\theta}\right)\right|^{-1} \tag{1.28}$$

Assuming a circular symmetry of the lens as in the figure 1.4: $\mu = \frac{\theta}{\theta_s}\frac{d\theta}{d\theta_s}$

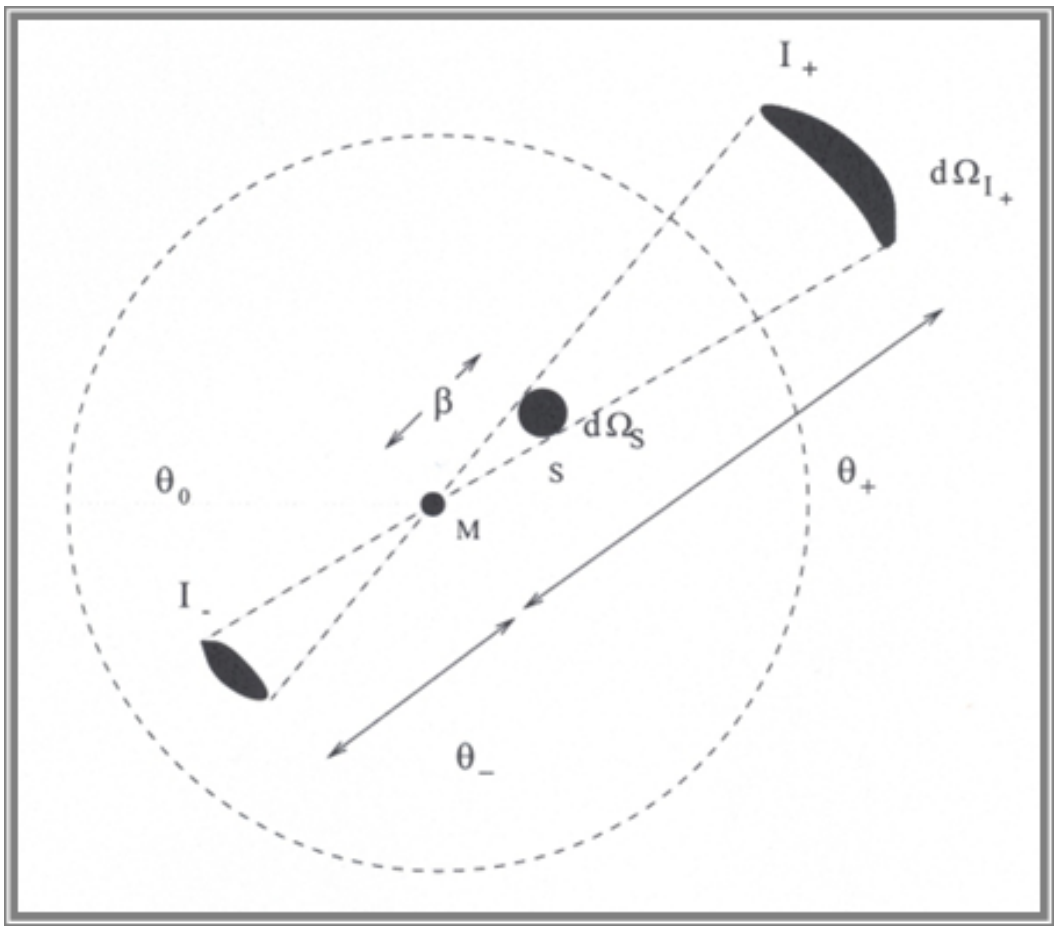

Fig. 1.4.: Illustration of a gravitational lens with magnification for a point source from [18]. β correspond to the angle between deflector and source which is θ_s in the previous demonstration.θ_- and θ_+ are respectively the demagnified and magnified images positions. The dotted circle corresponds to the Einstein ring position.

by considering $u = \frac{\theta_s}{\theta_E}$ the lens-image separation in units of Einstein ring radius, we get:

$$\mu_\pm = \frac{u^2+2}{2u\sqrt{u^2+4}} \pm \frac{1}{2} \tag{1.29}$$

The $+$ solution is always magnified while the $-$ solution can be magnified or demagnified depending on the value of u. If the source is inside the Einstein radius, $\mu > 1.34$.

Finally, the total magnification gives:

$$\mu = \mu_+ + \mu_- = \frac{u^2+2}{u\sqrt{u^2+4}} > 1 \tag{1.30}$$

For a point-like source, if $u \to 0$, $\mu \to \infty$. If $u \to \infty$, $\mu \to 1$. In the case of too-small image separation, the magnification can still be measured. This is used when the mass of the deflector is too small to dissociate the image from the lens. But it is also used when the image and the lens separation cannot be resolved and this technique is called micro-lensing.

1.3 Convolutional Neural Network to the rescue

With the era of large-scale surveys, Astrophysics has to deal with a huge amount of data and faces similar problems as the Big Data industry. As the amount of data grows, Machine learning and Deep learning field improved at the same time allowing the industry to manage the processing of those data.

The main type of data in Astrophysics is images and this is especially the case for the study of gravitational lenses. Automatically detecting gravitational lenses require methods able to detect localized features. Convolutional Neural Networks (CNN) are well-suited for this task. Convolution layers are able to detect local correlations with features learned from the data[19].

CNNs have proven their efficiencies in many fields as computer vision and self-driven cars [20] but also in research fields like medicine [21] and biology [22]. This is why so many attempts at auto-detection of gravitational lenses use CNNs. Obviously, there are other methods[23] investigated but CNNs are widely at the core of the research for strong lensed systems.[16][24][25][26][27].

1.4 A new approach

This work aims to explore innovative techniques to automate the detection of gravitational lenses. This time, CNNs will be discarded, but parametric and non-parametric models will be explored and combined with the power of other machine-learning methods. We will deeply explore one method but we will later discuss different ones that came to our mind.

One of the shortcomings of the CNN approach results in a loss of interpretability. Indeed, Neural networks are often considered black boxes even if we can intuitively understand what is going on inside of these black boxes. In this master thesis, we will mostly use a parametric model among many others: the Sersic model

[28] that has the advantage of being highly understandable. We will also use common non-parametric indices like Asymmetry, Concentration, Gini[29], and many more[30][31] that we will study later in this work. During this work, I needed a controlled framework that is not provided with real data. First, too few lensed galaxies cases are available nowadays. And next, the same lensed versus non-lensed galaxy is hard to obtain while it's highly relevant to my work. My dataset contains both non-lensed and simulated galaxy-galaxy strong gravitational lensing from true galaxy images. It ensures both control and proximity with true data. Section 2.1 will go deeply into the conception of the dataset.

One of the tricks in this work is to fit a Sersic model on a galaxy candidate and detect the presence of a lens thanks to the divergence to the non-lensed model. To well understand the idea of this method, a comparison of a fitted Sersic profile on a non-lensed galaxy and the same lensed galaxy is displayed in fig 1.5. Already in this figure, we can notice an increase of the amplitude I_e and a lower sersic index n. The effective radius R_{eff} is also decreased by the presence of the lens images. The sersic profile is mainly defined by 3 parameters: the amplitude I_e, the effective radius R_{eff}, and the sersic index n: $I(R) = I_e exp\left(-b_n\left[\left(\frac{R}{R_{eff}}\right)^{\frac{1}{n}} - 1\right]\right)$. From [32], $b_n = 1.9992n + 0.3271$ for $0.5 < n < 10$. We will thus constrain the non-lensed distribution of Sersic parameters; and in case a gravitational lens is present, the luminosity in the arms of the galaxy will increase and these parameters will diverge from the "standard" distribution enabling us to detect the lens. In the parameter space, we should observe a separation of point clouds allowing us to discriminate non-lensed from lensed galaxies. The same logic will be applied with many more parameters. A high Asymmetry should be present in the case of non-ring lenses. The same behavior for the Concentration and Gini indices is expected. Concentration is basically a ratio between radii containing 20% and 80% of the luminosity (ie: $C = 5log\left(\frac{r_{80}}{r_{20}}\right)$[29]), and we expect a higher r_{80} as lens images enhance the periphery of the galaxy. Because of the enhancement of the periphery, the Gini index which quantifies inequality in a population will increase, meaning a lower inequality in luminosity.

In this report, we will start by describing data. In a second time, we will focus on the methods used to perform this work. And before a conclusion, we will discuss our results and the other methods we could have used.

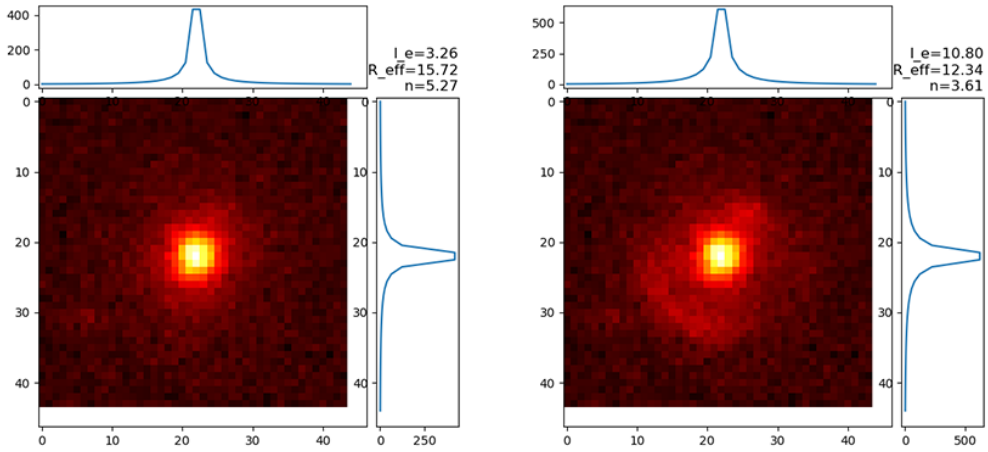

Fig. 1.5.: Comparison between fitted sersic profiles in the case of a non-lensed galaxy (left) and the sersic profile for the same galaxy with a lens (right).

2 Data

To test my method, I needed simulated data as discussed in section 1.4. Instead of making self-made simulated data, I worked with E. Savary, K. Rojas, M. Maus, et al dataset [26] which was a gain of time. In the frame of a PhD work, with longer-term deadlines, it could have been interesting to build my own dataset to get higher control over it. This dataset was made for a CNN-based application but it is suited to our framework. This part thus aims to explain the design of the dataset and have a better understanding of the data. The first step is to know how the dataset was collected and designed. The second step is to make a sanity check of the dataset and identify the different possible cases. And the last step is to identify the nature of the signal and the associated statistics.

2.1 Origin of the Data

A part of the images constituting our simulated dataset was acquired as part of the Canada France Imaging Survey (CFIS), which is a component of the Ultraviolet Near Infrared Optical Northern Survey (UNIONS). UNIONS is a Collaboration open to Canadian, French, and Japanese PhD students, astronomers, and members of the Pan-STARRS team. This collaboration aims to provide answers about dark matter, galactic to cluster scaled structures of the Universe, and the assembly of the Milkyway. This collaboration will contribute to ground-based photometry within the Euclid ESA space mission[1].

CFIS mainly uses the Canada-France-Hawaii Telescope (CFHT) to complete a survey of 8000 deg^2 of the northern sky in u photometric band (CFIS-u) and 4800 deg^2 in the r photometric band (CFIS-r). CFHT is a world-class 3.6 m optical/infrared telescope located on top of the Mauna Kea volcano in Hawaii[2]. It is equipped with MegaCam which is a wide-field optical imaging device built from 40 2048x4612 pixels CCD cells. MegaCam has a total of 380 Megapixels for a square Field-of-View (FoV) of 1 deg^2. The resolution of the telescope is 0.187 arcsecond/pixel.[3]

[1] https://www.skysurvey.cc/
[2] https://www.cfht.hawaii.edu/en/about/
[3] https://www.cfht.hawaii.edu/Science/CFIS/

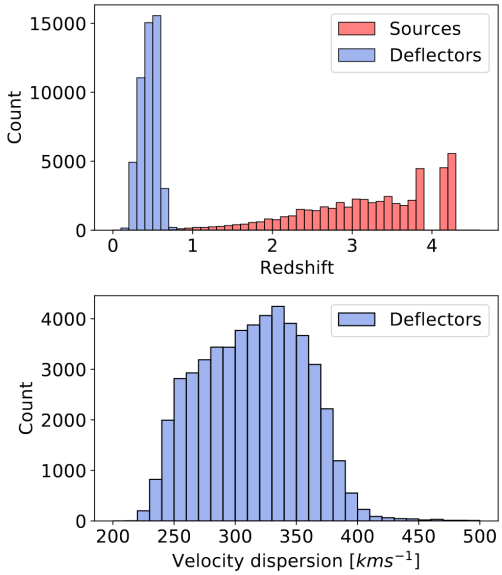

Fig. 2.1.: Redshit distribution of LRG galaxies (blue) and background lensed galaxies (red). The LRG velocity dispersion is important for Einstein radius computation (see 2.1 for more details). From [26]

The dataset we use is simulated images from real data coming from the CFIS Data Release 2 and HST/ACS F814W images. The way it is built is the following: CFIS images are used as deflectors galaxies (fig 2.2) and Hubble Space Telescope (HST) images lie in background sources that are lensed by software (fig 2.3). Images size is a square of 44 pixels which represents an FoV of 8.17". Images from CFIS are exclusively from CFIS-r data and more specifically Luminous Red Galaxies (LRG). These objects are expected to have the largest lensing cross section due to their bright and massive properties. Background galaxies were converted in the r photometric band with HSC ultra-deep stacked images. Images have an FoV of 10" for each side which corresponds to 0.03" per pixel.

Foreground galaxy images (LRG) have SDSS spectra allowing us to get access to velocity dispersion σ and a redshift z estimate available in the image headers (Image headers store metadata of the image). Background images which are all included in COSMOS2015 [33] and Galaxy Zoo catalog [34] were obtained using public spectroscopic catalogs or estimated from the best photometric redshift from [33]. According to figure 2.1, the foreground LRG galaxies spans the ranges $200 < \sigma < 500\ km\ s^{-1}$ and $0.1 < z < 0.7$. It is important to notice that already lensed LRG galaxies are present in the dataset but the effects on the performances of doubled lensed or misclassified images are considered negligible knowing the occurrence of the phenomenon (10^{-5}).

In this work, like in the reference paper, we will perform classification and thus train machine learning classifiers to identify gravitational lenses. To do so we define positive cases and negative cases. Negative cases are non-lensed galaxies randomly drawn from LRG galaxies sample described previously belonging to CFIS-r data. While positive cases are built from the combination of a foreground galaxy (CFIS) and a background-lensed galaxy (HST). The main steps of the design of positive cases follow these main steps:

- Random selection of an LRG
- Assignment of a singular isothermal ellipsoid mass model to the LRG galaxy.
- Random selection of a galaxy from HST sample
- Position of the source is randomly chosen with total magnification $\mu \geq 2$
- Computation of high-resolution image of the lensed source
- Convolution of the lensed source with the CFIS Point Spread Function (PSF)
- Combination of the deflector and the lensed source images

Let's go deeper into details about the different steps and the assumption and choices made during the process. The first assumption is the assignation of a mass profile model. The model used is the singular Isothermal Ellipsoid (SIE) model; a generalization of the singular isothermal sphere discussed in the section 1.2.3. This model is parameterized by five free parameters: Einstein radius, center coordinates of the lens, ellipticity, and position angle. Since every image was designed to host the deflector center at the center of the image, the center coordinates are a fixed value. The ellipticity and the position angle (PA) were derived from the second moment of the light profile of the LRG. In this model, it is assumed that the ellipticity and the PA derived from the light distribution are the same as the mass distribution profile.

This being done, a source galaxy is randomly selected within the HST sample. with the redshift information of both galaxies and the velocity dispersion, the Einstein radius is computed. Indeed, Luminosity and velocity dispersion are linked by the Faber-Jackson relation. The value of Einstein's radius (see equation 1.18) is imposed so that the angular size falls in the interval $0.8" < \theta_E < 3.0"$. The lower limit is chosen to prevent lens-galaxy blending while the upper limit is set to fit into the image frame. If those conditions are not met, another source galaxy is chosen until it the lens simulation fits the conditions. After 100 iterations the dispersion velocity of the deflector is increased by 50%. If the conditions are not met after this process, the deflector is discarded from the dataset. As explained in the paper [26], this

velocity dispersion boost involves a few objects with small velocity dispersion and it is not expected to introduce a significant morphological bias.

The next systematic choice made during the building process is the total magnification constraint. E. Savary, K. Rojas, M. Maus, et al decided to impose $\mu \geq 2$ because it coincides with the threshold for a multiple-image lens[35]. Setting a higher limit would have increased the number of full Einstein rings among the simulations and this could lead to an increase of false positives by mistaking ring galaxies.

When all those conditions are met, a high-resolution image of the lensed source is computed and convolved with the CFIS PSF. Here the HST Point spread function is neglected since it is sharper than the CFIS PSF. Before applying the CFIS PSF one, it is important to re-sample the PSF to the HST pixel size and then down-sampled to the CFIS pixel size after the convolution. The final step is the addition of the lensed source image to the foreground galaxy image.

2.2 Exploration of the dataset

Our dataset is made of multiple files divided into 5 types of data. We have first `LRG only` images which are the CFIS-r images visible in fig 2.2. The second type of image is `Lensed source only` images which are the lensed images of an HST source galaxies as shown in fig 2.3. The third photometric-based images are the combination of `LRG only` and `Lensed source only` images which gives `Lens simulation` images. Figure 2.4 represent those images which are the combination of images in fig 2.2 and 2.3. The two other types of data are PSF and RMS files. PSF files contain the two-dimensional function associated with the response of a focused imaging system (here the Canada France Hawaii Telescope) to a point source. We only get the PSF from CFHT but as mentioned in section 2.1 we neglected the HST PSF. Finally, RMS files correspond to Root Mean Square errors associated with each pixel. RMS files were built from weight maps computed from gain and relative normalization of noise using `SWarp`[4] software. It is important to note that we only get RMS files associated with `LRG only` images. We will see later how to generate RMS files for `Lens simulation` files. A sample of PSF and RMS files can be found in figures 2.5 2.6.

[4] `https://www.astromatic.net/software/swarp/`

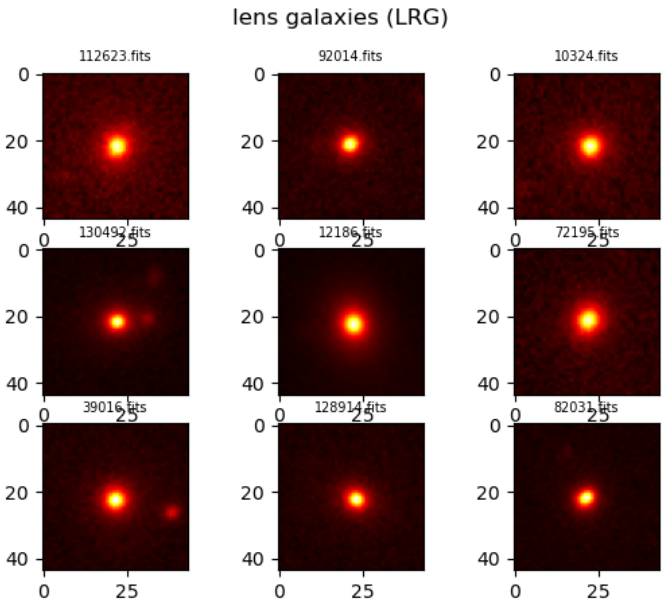

Fig. 2.2.: Sample of 9 images from the CFIS-r dataset. Those images are used as lens galaxies during the design of the dataset. Images are displayed with a linear red colormap.

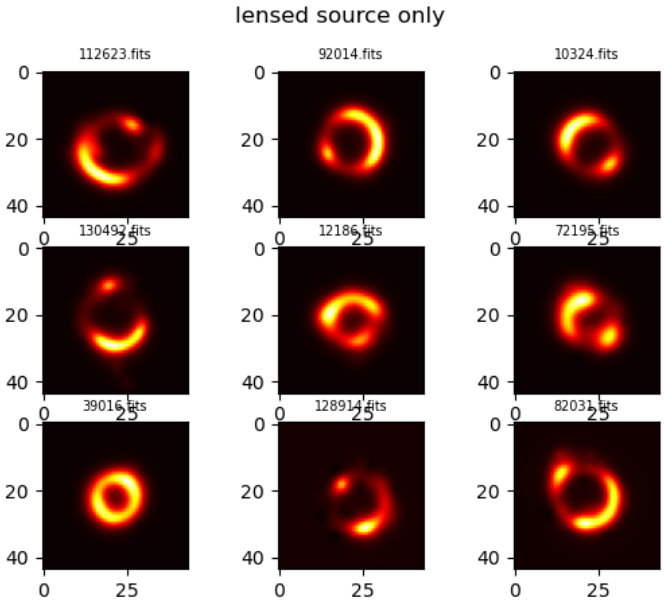

Fig. 2.3.: Sample of 9 simulated lens images from the HST source galaxies dataset. Those images are used as lens features during the design of the dataset. Images are simulated lenses according to lens galaxies displayed in fig 2.2.

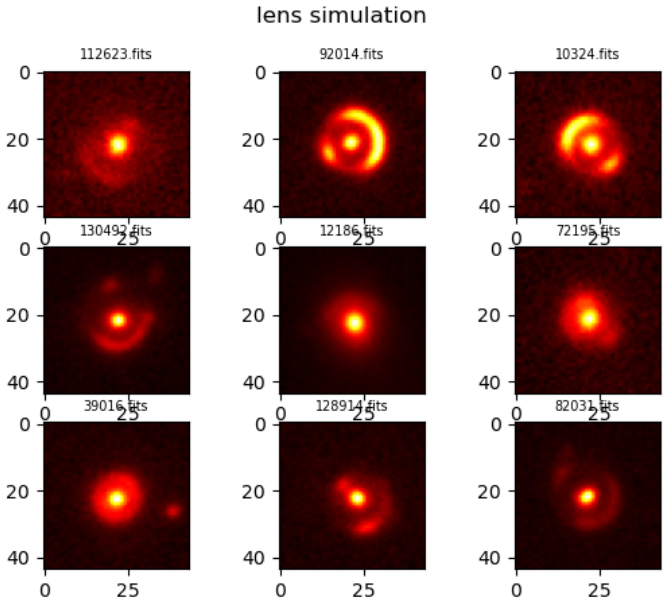

Fig. 2.4.: Sample of 9 simulated images from the CFIS-r and HST dataset. Those images are addition of fig 2.2 and 2.3 images.

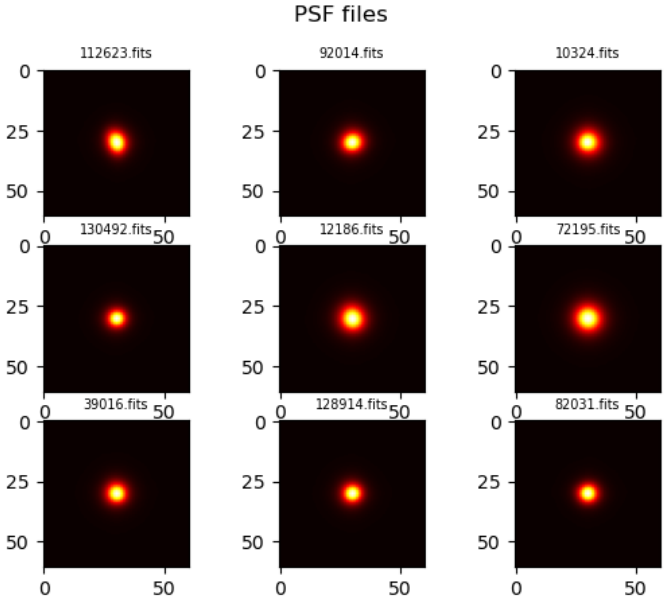

Fig. 2.5.: Sample of 9 PSF images from the Canada France Hawaii Telescope.

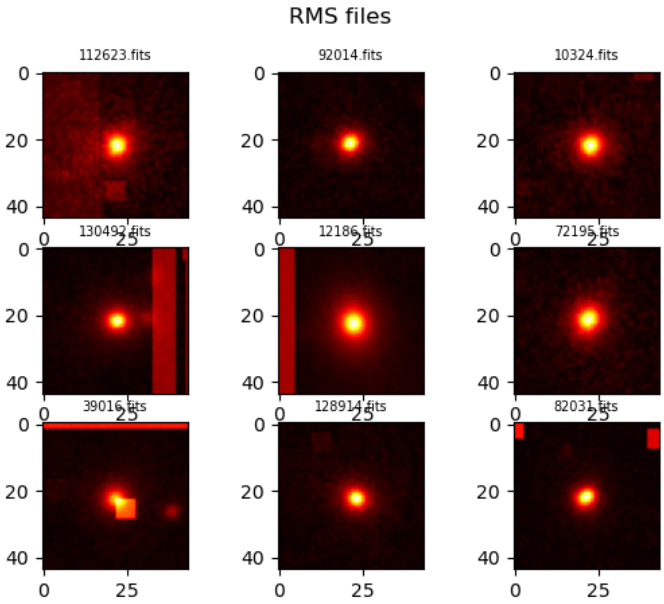

Fig. 2.6.: Sample of 9 RMS images associated with CFIS-r images. Squares on some images result from a mask of satellite tracks, cosmic rays or dead pixels.

2.3 Noise and signal

Imaging galaxies is not as simple as taking photographs in daily photography. Imaging deep sky objects implies low light intensity where different noises become non-negligible. Those noises arise due to different physical phenomena that we won't emphasize here because they have been corrected already. However, we will focus on the photon noise which persists in data and cannot be canceled with calibration files so it is important to quantify it.

The photon noise is linked to the physical nature of the light and affects the quality of the data. This phenomenon is not perceptible by the human eye because of the retinal persistence that cancels irregularities in the photonic flux. The flux of photons is a random variable that is associated with a counting problem. The statistics associated with a counting phenomenon are modeled by Poisson distribution. We can thus evaluate the noise $\sigma_{photons}$ by the following equation, where N is the number of detected photons:

$$\sigma_{photons} \propto \sqrt{N} \tag{2.1}$$

Pixel Intensities are expressed as ADU units which means Analog-to-Digital-Units. One can easily switch from ADUs to the number of electrons thanks to the gain $g = \frac{number\ of\ electrons}{ADU}$. We can thus link the intensity in ADU to the intensity in electron I_e units with the gain g.

$$I_{ADU} = I_e \times g \tag{2.2}$$

Thanks to equation 2.1, $I_e = \sigma_e^2 = RMS^2$ and we then get the following relation:

$$RMS^2 = \frac{I_{ADU}}{g} \tag{2.3}$$

In our case, we can consider that the image is made of photons from the object of interest and photons coming from the background sky $I_{ADU} = I_{obj,ADU} + I_{sky,ADU}$. In object regions and their neighborhood, the intensity of the sky is very low or even negligible compared to the object intensity and $I_{ADU} \approx I_{obj,ADU}$ And the total Root Mean Square error is :

$$TOTAL\ RMS^2 = \sigma_{obj}^2 + \sigma_{sky}^2 \approx \frac{I_{ADU}}{g} + \sigma_{sky}^2 \tag{2.4}$$

It is important to notice that in regions away from an object, $I_{sky,ADU} \approx 0$ and $TOTAL\ RMS^2 \approx \sigma_{sky}^2$

If `LRG only` images are well background substracted, we expect the relation 2.4 to fit to the data. In order to check that, let's fit this linear relation on plotted pixel values (in ADU) as a function of RMS^2 as it can be found in fig 2.7. Before discussing the results of this graph, let's focus on the general trend and features of the point clouds only. As discussed a few lines earlier, lower values of pixels, imply a dominant background noise and lead to a plateau that is present in fig 2.8. It is common to find profiles as displayed in fig 2.9 with points away from the point cloud with the same trend but translated along the y-axis. It is due to one or several masks present in the RMS file increasing error bars in case of a polluting source like satellite tracks, cosmic rays, or even dead pixels.

To enhance the accuracy of the fit of relation 2.4 on the point cloud, I discarded points belonging to the plateau at low pixel values. However, we will also evaluate the background noise by only considering points of this plateau. So, a sample of 10 fits is displayed in fig 2.7, and values of the computed gain and computed σ_{sky}^2 with different techniques are available in table 2.1.

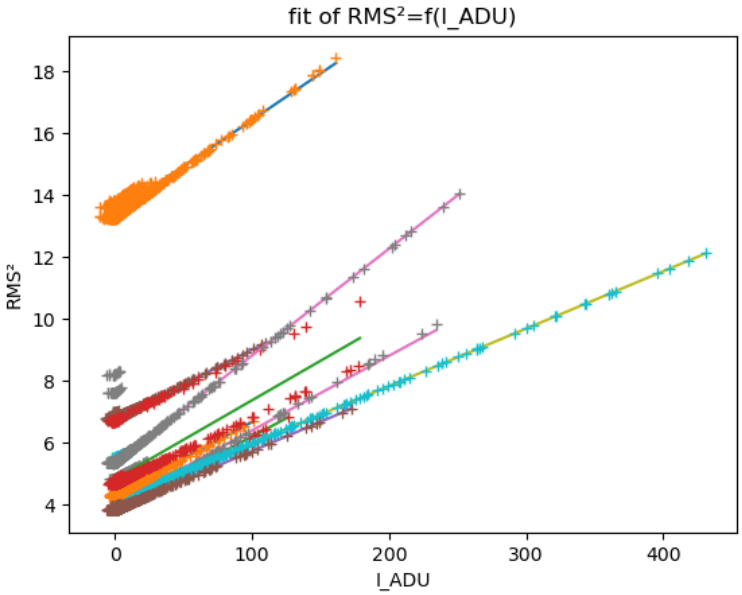

Fig. 2.7.: Linear regression of 9 `LRG only` RMS^2 as a function of pixel intensity in ADU using relation 2.4.

Fitted gain values are compared to the gain values available in the image headers. For σ^2_{sky} we compared fitted values with the evaluated mean value of the so-called plateau. I also evaluated it by another method that I call the corner method. The corner method consists in taking some pixel values at the 4 corners of the image where the background is dominant. I took a square kernel of 5 pixels large at each corner so we have a total of 100 pixels. To obtain the background noise, I took the squared standard deviation of those pixels.

Coming back to table 2.1 results, we clearly see that the gain values computed are coherent with the ones found in image headers and we also have the same evaluations for the background noise. It is particularly true between the fit and the plateau method. However, corner methods only consider 100 pixels which is a small sample of the total background sky, and can thus not confidently evaluate σ^2_{sky}. Moreover, there is a non-zero probability that a contaminating neighbor source (galaxy or star) is located in the corner which should have an effect on this estimation.

In the following of this work, we will need RMS files for `Simulated images`, but we only have RMS files for `LRG only` images. Now that we know a bit more about the link between the signal and the noise, it is easy to build a new RMS file for `Simulated images`. But before that, I checked that images are a simple addition of `LRG only` and `Lensed source only` images by substracting both files from the

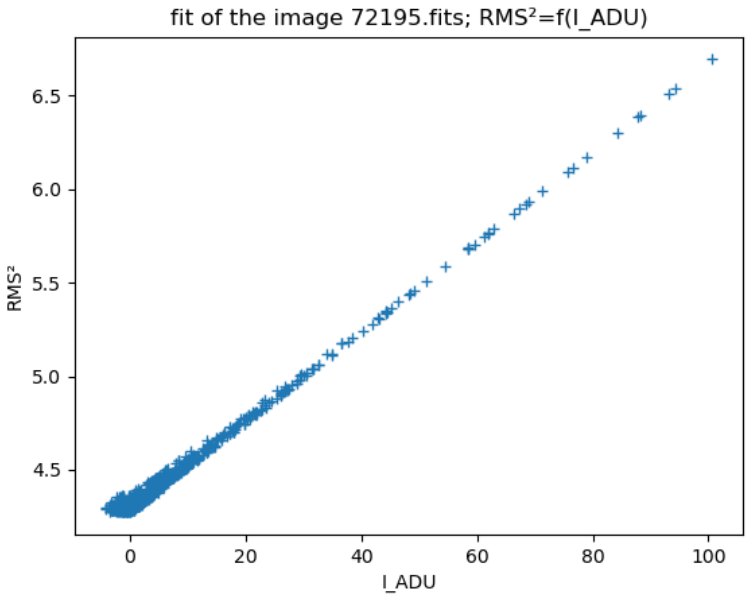

Fig. 2.8.: RMS^2 as a function of pixel intensity in ADU for `LRG only` images

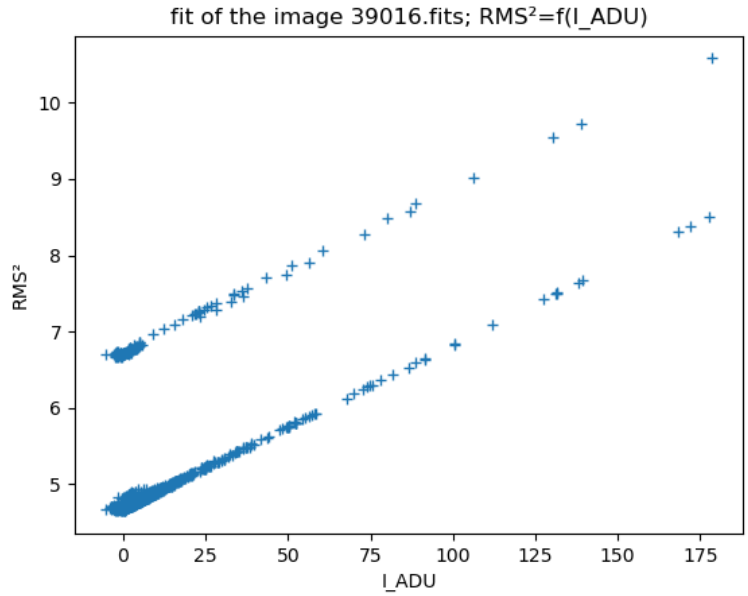

Fig. 2.9.: Pixel value in ADU as a function of RMS^2 for `LRG only` images with polluting source and RMS mask.

computed gain (fit)	real gain	σ^2_{sky} (fit)	σ^2_{sky} (plateau)	σ^2_{sky} (corner method)
33.27	31.58	13.43	13.56	12.12
42.36	42.36	3.84	3.88	3.19
44.79	44.49	6.77	6.81	4.00
41.43	39.04	3.98	4.11	2.72
53.92	53.97	4.12	4.58	9.35
42.12	41.83	4.29	4.35	3.73
39.16	46.55	4.82	4.86	2.78
52.78	52.75	3.83	3.88	3.53
28.93	29.03	5.36	5.48	4.16

Tab. 2.1.: Comparison of values computed for the gain and the background noise. fit values stand for values computed thanks to linear regression, plateau by tacking the mean value of the plateau and corner method by the method described in section 2.3. The real gain is the one available in the image header.

simulated one. So based on equation 2.3, I reconstructed the RMS file with the quadratic sum of the already existing RMS file and a computed Mean Square error using the gain value available in the `LRG only` headers. Here is the expression of the new RMS:

$$RMS_{reconstructed} = \sqrt{RMS^2 + \frac{I_{ADU,Lensed\_source\_only}}{g_{LRG}}} \tag{2.5}$$

Bibliography

[1] I. Newton, *Optiks or a Treatise of the Reflexions, Refractions, Inflexions Colours of Light*. 1704, Book 3, Part 1, Querie 1 (cit. on p. 1).

[2] R. McCormmach, "John michell and henry cavendish: Weighing the stars," vol. 4, no. 2, pp. 126–155, Dec.1968 (cit. on p. 1).

[3] K.-H. Lotze and S. Simionato, "Henry Cavendish and the effect of gravity on propagation of light: A postscript," *The European Physical Journal H*, vol. 46, no. 1, p. 24, Sep. 2021 (cit. on p. 1).

[4] Wikisource. "Translation:on the deflection of a light ray from its rectilinear motion — wikisource." [Online; accessed 7-November-2022]. (2021), [Online]. Available: `https://en.wikisource.org/w/index.php?title=Translation:On_the_Deflection_of_a_Light_Ray_from_its_Rectilinear_Motion&oldid=10821714` (cit. on p. 1).

[5] A. Einstein. "On the influence of gravitation on the propagation of light." [Online; accessed 7-November-2022]. (1911), [Online]. Available: `https://einsteinpapers.press.princeton.edu/vol3-trans/393` (cit. on p. 1).

[6] J.-M. Ginoux, "Albert einstein and the doubling of the deflection of light," *Foundations of Science*, vol. 27, pp. 1–22, Feb. 2021 (cit. on p. 1).

[7] E. S. A. Dyson Frank Watson and D. C., "Ix. a determination of the deflection of light by the sun's gravitational field, from observations made at the total eclipse of may 29, 1919," *Philosophical Transactions of the Royal Society of London.*, vol. Series A, Containing Papers of a Mathematical or Physical Character, no. 220, pp. 291–333, 1920 (cit. on p. 1).

[8] F. Zwicky, "Nebulae as gravitational lenses," *Phys. Rev.*, vol. 51, pp. 290–290, 4 Feb. 1937 (cit. on pp. 1, 2).

[9] R. C. C. Dennis Walsh and R. Weymann, "0957 + 561 a, b: Twin quasistellar objects or gravitational lens?" *Nature*, vol. 279, pp. 381–384, 1979 (cit. on p. 1).

[10] T. York, N. Jackson, I. W. A. Browne, *et al.*, "CLASS B0631+519: last of the Cosmic Lens All-Sky Survey lenses,", vol. 361, no. 1, pp. 259–271, Jul. 2005. arXiv: `astro-ph/0505093 [astro-ph]` (cit. on p. 2).

[11] Y. Tsapras, "Microlensing searches for exoplanets," *Geosciences*, vol. 8, no. 10, p. 365, Sep. 2018 (cit. on p. 2).

[12] R. Massey, T. Kitching, and J. Richard, "The dark matter of gravitational lensing," *Reports on Progress in Physics*, vol. 73, no. 8, p. 086 901, Jul. 2010 (cit. on p. 2).

[13]R. S. Ellis, "Gravitational lensing: A unique probe of dark matter and dark energy," *Philosophical Transactions of the Royal Society A: Mathematical, Physical and Engineering Sciences*, vol. 368, no. 1914, pp. 967–987, 2010. eprint: https://royalsocietypublishing.org/doi/pdf/10.1098/rsta.2009.0209 (cit. on p. 2).

[14]W. J., "Gravitational lensing in astronomy.," *Living reviews in relativity,*, vol. 1, 1998 (cit. on p. 2).

[15]T. E. Collett, "The population of galaxy–galaxy strong lenses in forthcoming optical imaging surveys," *The Astrophysical Journal*, vol. 811, no. 1, p. 20, Sep. 2015 (cit. on p. 3).

[16]E. Zaborowski, A. Drlica-Wagner, F. Ashmead, *et al.*, *Identification of galaxy-galaxy strong lens candidates in the decam local volume exploration survey using machine learning*, 2022. arXiv: 2210.10802 [astro-ph.GA] (cit. on pp. 3, 10).

[17]J.-F. Claeskens and J. Surdej, "Gravitational lensing in quasar samples," *The Astronomy and Astrophysics Review*, vol. 10, no. 4, pp. 263–311, Mar. 2002 (cit. on p. 3).

[18]P. Magain. "Extragalactic distances." [Online; accessed 24-May-2023]. (2023), [Online]. Available: http://www.astro.ulg.ac.be/cours/magain/AstrophysiqueExtragal/Extragal01E.ppt (cit. on pp. 3, 9).

[19]L. Alzubaidi, J. Zhang, A. J. Humaidi, *et al.*, "Review of deep learning: Concepts, CNN architectures, challenges, applications, future directions," *Journal of Big Data*, vol. 8, no. 1, p. 53, Mar. 2021 (cit. on p. 10).

[20]M. Saranya, N. Archana, J. Reshma, S. Sangeetha, and M. Varalakshmi, "Object detection and lane changing for self driving car using cnn," in *2022 International Conference on Communication, Computing and Internet of Things (IC3IoT)*, 2022, pp. 1–7 (cit. on p. 10).

[21]B. Kayalibay, G. Jensen, and P. van der Smagt, *Cnn-based segmentation of medical imaging data*, 2017. arXiv: 1701.03056 [cs.CV] (cit. on p. 10).

[22]M. F. Aslan, K. Sabanci, A. Durdu, and M. F. Unlersen, "COVID-19 diagnosis using state-of-the-art CNN architecture features and Bayesian Optimization," *Computers in Biology and Medicine*, vol. 142, p. 105 244, 2022 (cit. on p. 10).

[23]S. Madireddy, N. Ramachandra, N. Li, *et al.*, *A modular deep learning pipeline for galaxy-scale strong gravitational lens detection and modeling*, 2022. arXiv: 1911.03867 [astro-ph.IM] (cit. on p. 10).

[24]S. Rezaei, J. P. McKean, M. Biehl, W. de Roo, and A. Lafontaine, "A machine learning based approach to gravitational lens identification with the International LOFAR Telescope," *Monthly Notices of the Royal Astronomical Society*, vol. 517, no. 1, pp. 1156–1170, Nov. 2022 (cit. on p. 10).

[25]J. Pearson, C. Pennock, and T. Robinson, "Auto-detection of strong gravitational lenses using convolutional neural networks," en, *Emergent Scientist*, vol. 2, p. 1, 2018, Publisher: EDP Sciences (cit. on p. 10).

[26]E. Savary, K. Rojas, M. Maus, *et al.*, "A search for galaxy-scale strong gravitational lenses in the Ultraviolet Near Infrared Optical Northern Survey (UNIONS)," Tech. Rep., Oct. 2021, Publication Title: arXiv e-prints ADS Bibcode: 2021arXiv211011972S Type: article (cit. on pp. 10, 13–15).

[27]C. Jacobs, T. Collett, K. Glazebrook, *et al.*, "An extended catalog of galaxy–galaxy strong gravitational lenses discovered in des using convolutional neural networks," *The Astrophysical Journal Supplement Series*, vol. 243, no. 1, p. 17, Jul. 2019 (cit. on p. 10).

[28]J. L. Sérsic, "Influence of the atmospheric and instrumental dispersion on the brightness distribution in a galaxy," *Boletin de la Asociacion Argentina de Astronomia La Plata Argentina*, vol. 6, pp. 41–43, Feb. 1963 (cit. on p. 11).

[29]J. M. Lotz, J. Primack, and P. Madau, "A New Nonparametric Approach to Galaxy Morphological Classification,", vol. 128, no. 1, pp. 163–182, Jul. 2004. arXiv: astro-ph/0311352 [astro-ph] (cit. on p. 11).

[30]M. A. Peth, J. M. Lotz, P. E. Freeman, *et al.*, "Beyond spheroids and discs: classifications of CANDELS galaxy structure at $1.4 < z < 2$ via principal component analysis,", vol. 458, no. 1, pp. 963–987, May 2016. arXiv: 1504.01751 [astro-ph.GA] (cit. on p. 11).

[31]P. E. Freeman, R. Izbicki, A. B. Lee, *et al.*, "New image statistics for detecting disturbed galaxy morphologies at high redshift,", vol. 434, no. 1, pp. 282–295, Sep. 2013. arXiv: 1306.1238 [astro-ph.CO] (cit. on p. 11).

[32]A. W. Graham and S. P. Driver, "A concise reference to (projected) sérsic r1/n quantities, including concentration, profile slopes, petrosian indices, and kron magnitudes," *Publications of the Astronomical Society of Australia*, vol. 22, no. 2, pp. 118–127, 2005 (cit. on p. 11).

[33]C. Laigle, H. J. McCracken, O. Ilbert, *et al.*, "THE COSMOS2015 CATALOG: EXPLORING THE 1 &lt iz/i &lt 6 UNIVERSE WITH HALF a MILLION GALAXIES," *The Astrophysical Journal Supplement Series*, vol. 224, no. 2, p. 24, Jun. 2016 (cit. on p. 14).

[34]R. E. Hart, S. P. Bamford, K. W. Willett, *et al.*, "VizieR Online Data Catalog: Galaxy Zoo 2: new classification (Hart+, 2016)," *VizieR Online Data Catalog*, J/MNRAS/461/3663, J/MNRAS/461/3663, Nov. 2017 (cit. on p. 14).

[35]G. P. Smith, A. Robertson, G. Mahler, *et al.*, "Discovering gravitationally lensed gravitational waves: predicted rates, candidate selection, and localization with the Vera Rubin Observatory," *Monthly Notices of the Royal Astronomical Society*, vol. 520, no. 1, pp. 702–721, Jan. 2023. eprint: https://academic.oup.com/mnras/article-pdf/520/1/702/49032005/stad140.pdf (cit. on p. 16).

List of Figures

List of Tables

List of Listings

Example Appendix

A

Hello, here is some text without a meaning. This text should show what a printed text will look like at this place. If you read this text, you will get no information. Really? Is there no information? Is there a difference between this text and some nonsense like “Huardest gefburn”? Kjift – not at all! A blind text like this gives you information about the selected font, how the letters are written and an impression of the look. This text should contain all letters of the alphabet and it should be written in of the original language. There is no need for special content, but the length of words should match the language.

A.1 Appendix Section 1

This is the second paragraph. Hello, here is some text without a meaning. This text should show what a printed text will look like at this place. If you read this text, you will get no information. Really? Is there no information? Is there a difference between this text and some nonsense like “Huardest gefburn”? Kjift – not at all! A blind text like this gives you information about the selected font, how the letters are written and an impression of the look. This text should contain all letters of the alphabet and it should be written in of the original language. There is no need for special content, but the length of words should match the language.

Alpha	Beta	Gamma
0	1	2
3	4	5

Tab. A.1.: This is a caption text.

A.2 Appendix Section 2

And after the second paragraph follows the third paragraph. Hello, here is some text without a meaning. This text should show what a printed text will look like

at this place. If you read this text, you will get no information. Really? Is there no information? Is there a difference between this text and some nonsense like “Huardest gefburn”? Kjift – not at all! A blind text like this gives you information about the selected font, how the letters are written and an impression of the look. This text should contain all letters of the alphabet and it should be written in of the original language. There is no need for special content, but the length of words should match the language.

Alpha	Beta	Gamma
0	1	2
3	4	5

Tab. A.2.: This is a caption text.

After this fourth paragraph, we start a new paragraph sequence. Hello, here is some text without a meaning. This text should show what a printed text will look like at this place. If you read this text, you will get no information. Really? Is there no information? Is there a difference between this text and some nonsense like “Huardest gefburn”? Kjift – not at all! A blind text like this gives you information about the selected font, how the letters are written and an impression of the look. This text should contain all letters of the alphabet and it should be written in of the original language. There is no need for special content, but the length of words should match the language. Hello, here is some text without a meaning. This text should show what a printed text will look like at this place. If you read this text, you will get no information. Really? Is there no information? Is there a difference between this text and some nonsense like “Huardest gefburn”? Kjift – not at all! A blind text like this gives you information about the selected font, how the letters are written and an impression of the look. This text should contain all letters of the alphabet and it should be written in of the original language. There is no need for special content, but the length of words should match the language.

Colophon

This thesis was typeset with LaTeX 2_ε. It uses the *Clean Thesis* style developed by Ricardo Langner. The design of the *Clean Thesis* style is inspired by user guide documents from Apple Inc.

Download the *Clean Thesis* style at `http://cleanthesis.der-ric.de/`.

Declaration

You can put your declaration here, to declare that you have completed your work solely and only with the help of the references you mentioned.

, June 2023

Laisney Clément